Catalysis Science & Technology

Accepted Manuscript

ROYAL SOCIETY OF CHEMISTRY

www.rsc.org/catalysis

Journal Name

RSCPublishing

ARTICLE

Theoretical studies on the mechanism for the oxygen reduction reaction on clean and O-substituted Ta_3N_5(100) surfaces

Cite this: DOI: 10.1039/x0xx00000x

Received 00th January 2012,
Accepted 00th January 2012

DOI: 10.1039/x0xx00000x

www.rsc.org/

Eriko Watanabe, Hiroshi Ushiyama*, Koichi Yamashita,

The reaction mechanism for the oxygen reduction reaction (ORR) on Ta_3N_5(100) surfaces was examined theoretically. In particular, the effects of O-substitution on the catalytic activity have been discussed. First, the adsorption energy and geometry of an oxygen molecule adsorbed on a clean and O-substituted Ta_3N_5(100) surfaces were calculated. Energy diagrams for 2-electron and 4-electron reactions on the clean and O-substituted Ta_3N_5(100) surfaces were then examined. The results show that the adsorption energy of an oxygen molecule on the clean Ta_3N_5(100) surface is almost zero and the oxygen molecule is easier to adsorb on the O-substituted surface. However, OH and H_2O adsorb strongly on the O-substituted surfaces so that their desorption can be the rate-determing step. To improve the ORR activity, both O_2 and OH adsorption energy should be tuned. By the analysis of energy level of adsorbates and Ta_3N_5 O-substituted surface, the impurity state of Ta_3N_5 is the key descriptor for the adsorption energy. Therefore, the ORR activity can be controlled by changing the energy of the impurity state.

Introduction

The oxygen reduction reaction (ORR) and oxygen evolution reaction (OER) are the key reactions in both the cathode reaction of polymer electrolyte fuel cells (PEFCs) and the photo(electro)catalytic water-splitting reaction, respectively. In PEFCs, the ORR is the cathode reaction and the large overpotential of the ORR is the main cause for decreased efficiency[1]. Thus, to overcome the large overpotential, platinum catalysts are used. There have been numerous studies to clarify the mechanism for the ORR on Pt catalysts[2-5]. However, platinum is the precious metal that limits the widespread use of PEFCs; therefore, low-platinum or non-platinum catalysts for the ORR have been required, and various types of catalysts have been reported[6]. For example, as low platinum catalysts, alloy of Pt[7,8], core-shell structure with core of abundant metals[9], and Pt supported on nano-structuring carbon such as carbon nano-tubes[10] have been examined to reduce the amount of Pt used. As non-platinum catalysts, Fe and Co complex catalysts[11-14], carbon based catalysts[15-21], transition metal oxides, nitrides, and oxynitride catalysts[22-35], such as Ta_3N_5, TaNO, TaCNO, ZrO_xN_y, and NbO_xN_y, have been reported. Among all, transition metal oxide, nitride and oxynitride catalysts have an advantage of being stable in an acid environment[28,30] and are the promising materials for ORR non-platinum catalysts.

In the case of the photo(electro)catalytic water-splitting reaction, transition metal nitrides and oxinitrides have attracted much interest as well for promotion of the water-splitting reaction under visible light conditions[36]. Among them, Ta_3N_5 is one of the most promising materials because of the band gap of 2.1 eV suitable for the visible light absorption and its conduction band (CB) and valence band (VB) position straddling the H^+/H_2 and O_2/H_2O redox potential[37-39]. Therefore, research on Ta_3N_5 has focused on its optical properties and there have been fewer reports on the surface reactions of Ta_3N_5. However, OER is the reverse reaction of ORR, so that if the reaction site for ORR on Ta3N5 surface is effective, the OER in photocatalytic water-splitting can be promoted on the same site. Therefore, control of the ORR is the major issue to achieve a hydrogen energy system and the investigation of the ORR on Ta3N5 is useful for the improvement of both fuel cells and water-splitting systems.

Our research focus is improving the ORR activity on Ta_3N_5 by clarifying the reaction mechanism for oxygen reduction. Surface reactions on Ta_3N_5 have been reported partially, such as oxygen adsorption[40] and water adsorption[41], however, a fully calculated energy diagram of the ORR is reported for the first time in this paper. It is reported by XPS experiments that surface of Ta_3N_5 is so oxidized that the ratio of surface oxygen atom and nitrogen atom is almost 1:1 after synthesis[28]. It is also reported that such O-substitution to surface N atoms is thermodynamically stable in both bulk and surface region from DFT calculations[40,42]. Therefore we analysed the mechanism of oxygen reduction reaction on clean and O-substituted Ta_3N_5.

We have previously examined the stability and reactivity of Ta_3N_5 using density functional theory (DFT) calculations and shown that the (100) surface is the most stable surface, and that surface defects such as surface O-substitution have a significant effect on the surface reactivity[40]. Following this previous work, the reaction mechanism of oxygen reduction on Ta_3N_5(100) is examined here, and the effect of surface O-substitution on the ORR activity is discussed by comparison

of the reaction on clean and O-substituted Ta_3N_5(100) surfaces. We also discuss how to improve the ORR activity on Ta_3N_5 surface.

Computational Method

DFT calculations were performed using the SIESTA code[43]. The exchange correlation energy was calculated with a generalized gradient approximation (GGA) using the RPBE functional[44]. A double-z split-valence basis set with polarization orbitals for all elements[45] and norm-conserving pseudopotentials proposed by Troullier and Martins[46] were used. Spin polarized calculations were performed on all the system in our calculations. Geometry optimization was performed until the maximum atomic force was smaller than 0.02 eV/Å. The transition state was calculated using the nudged elastic band (NEB) method[47-49]. Ta_3N_5 is known to have pseudobrookite structure. It has orthohomobic/Cmcm group including 32 atoms in its unit cell[50]. The optimized size of the Ta_3N_5 unit cell was a=3.99 Å, b=10.69 Å, c=10.69 Å, where each lattice parameter almost matches the experimental data[50] (a=3.88 Å, b=10.21 Å, c=10.26 Å). Because of the relatively large lattice constants to b and c directions, the slab model was made by piling three Ta_3N_5 unit cells to *x* direction with 20 Å thick vacuum space (a=30.0 Å, b=10.21 Å, c=10.26 Å). This model is equivalent to the 6-layer model in ref. 40. The 6-layer slab model is sufficiently thick to represent the surface state because the model shows good convergence of both band gap and surface energy[40]. The energies were sampled on (1×2×2) grid with the Monkhorst-Pack method[51] which shows the total energy convergence within 1 meV/atom.

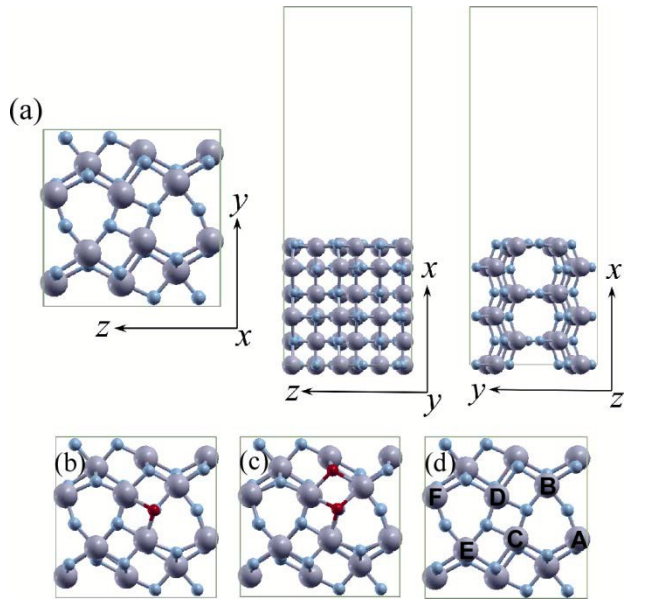

Figure 1. The Ta_3N_5 (100) structures of (a) clean surface from x, y and z directions (b) O1-substituted surface from x direction, (c) O2-substituted surface from x direction and (d) labeling of surface six Ta atoms in unit cell from x direction. The big purple atoms are Ta, small blue atoms are N and small red atoms are O.

The oxygen adsorption and the following reaction were examined using one reaction site per 6-layer model which corresponds to the coverage of 0.88 molecule/nm^{-2}. Although there is no direct comparable experimental data, the O_2 temperature-programmed desorption (TPD) on TiN and Pt show the O_2 adsorption density of 0.18-0.57 molecule/nm^{-2} on TiN and 2.1 molecule/nm^{-2} on Pt[24]. Thus, the difference of our calculation model and the experimental adsorption density is considered to be small. To make the O-substituted surfaces, one (O1-substituted surface) or two (O2-substituted surface) of the surface nitrogen atoms are replaced by oxygen atoms. The structures of clean, O1-substituted and O2-substituted surfaces are shown in Figure 1(a)-(c). On the clean surface, Ta sites in the unit cell are labelled from A to F, as shown in Figure 1(d). Sites A, C, D and F are geometrically equivalent, as are sites B and E. Calculations were performed using supercomputers at the Institute for Solid State Physics (ISSP), University of Tokyo.

Results and Discussion

3.1 Surface Structures and Oxygen Adsorption Structures

As the first elementary step of the ORR, oxygen adsorption on clean and O-substituted surfaces was examined, assuming molecular adsorption. The structures of molecular adsorption are classified into three types: Pauling-type (end-on adsorption), Griffiths-type (side-on adsorption on one surface atom), and Yeager-type (side-on bridge adsorption between two surface atoms). The examples of three type's oxygen adsorption structures on O2-substituted surface were pictured in Figure 2. Considering the symmetry, the energies for Pauling-type and Griffiths-type adsorption were calculated only for sites A and B for a clean surface, while the energies of Yeager-type adsorption were calculated between the A-B, A-C and C-D sites. On O-substituted surfaces, the symmetry was broken due to the O-substitution and the adsorption energies for the three-types of structures were calculated for every possible site. We assumed that strong oxygen adsorption sites can be active sites for the ORR.

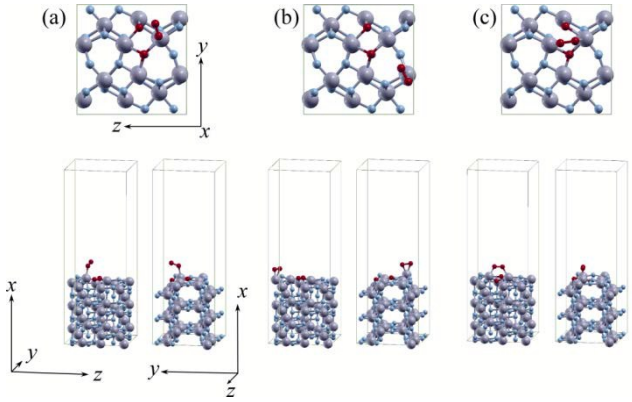

Figure 2. The structures of oxygen molecular adsorption of (a) Pauling-style at B site, (b) Griffiths-style at A site, and (c) Yeager-style between B and D on O2-substituted surface from three directions. The big purple atoms are Ta, small blue atoms are N and small red atoms are O.

The adsorption energy is defined as

$E_{ad} = E(\text{surf} + O_2) - \{E(\text{surf}) + E(O_2)\}$,

where $E(\text{surf} + O_2)$, $E(\text{surf})$, $E(O_2)$ are the respective energies of the surface with adsorbed O_2, only the surface, and O_2 itself. The negative value of E_{ad} means that the adsorption of oxygen on the surface is exothermic. The theoretically obtained

adsorption energies for Pauling-type and Griffiths-type adsorption on clean and O-substituted surfaces are shown in Table 1(a). The adsorption energies for Yeager-type adsorption were also calculated and are listed in Table 1(b).

The adsorption energies on the clean surface range from 0.05 to -0.06 eV in Table 1. Therefore, the oxygen molecules cannot adsorb at any sites on the clean surface. However, oxygen molecules can adsorb strongly on both the O1-substituted and O2-substituted surfaces because all E_{ad} in Table 1 are negative. Here we investigated the relationship between the adsorption energies and the number of substituted oxygen atoms for Pauling-type, Griffiths-type and Yeager-type adsorption. A comparison of the energy distribution on clean, O1-substituted and O2-substituted surfaces indicated that oxygen molecules strongly adsorb when the number of surface substituted oxygen atoms increases.

Next, the adsorption energies of each adsorption type were compared. The results of both O1-substitued and O2-substituted surfaces show that oxygen molecules with the Griffiths-type structure adsorb stronger than those with the Pauling-type structure. This is because one Ta-O bond is formed in Pauling-type adsorption, whereas two Ta-O bonds are formed in Griffiths-type adsorption. The activation energy of the structural change from Pauling-type adsorption to Griffiths-type adsorption on B and C sites was examined on O1-substituted and O2-substituted surfaces. The calculated activation energy is as large as 0.3 eV. The adsorption energies of Pauling-type structures are weaker than those of Griffiths-type structures and the activation energies from Pauling-type to Griffiths-type adsorption is not so high; therefore, we consider that all Pauling-type adsorption changes to Griffiths-type adsorption on every site. In the case of Yeager-type adsorption, oxygen molecules can adsorb on every site on O1-substituted and O2-substituted surfaces. Figure 3 shows the relationship between the adsorption energy and Ta-Ta bond length. From the analysis, oxygen molecules were determined to strongly adsorb between closely located

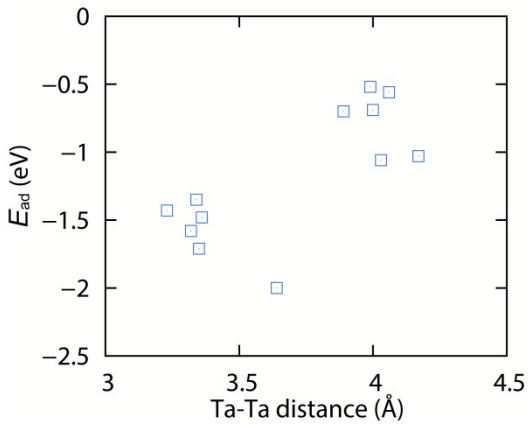

Figure 3. Adsorption energies of Yeager-type structure on O2-substituted surface are shown as a function of the distance between adsorption sites of two Ta atoms.

Ta atoms. The same trend can be seen on O1-substituted surface as well (see Table 1(b)). From analysis of oxygen adsorption on O-substituted surfaces, two types of adsorption sites were determined to be possible active sites. One is Yeager-type adsorption between two closely located Ta atoms, and the other is Griffiths-type adsorption on every Ta atom in the O-substitution structure. Therefore, we consider that the ORR starts from these two types of O_2 adsorption.

From experiments, O_2 adsorption was reported by TPD. The estimated O_2 adsorption energy of Ta_3N_5 nanoparticle is about 0.3 eV (desorption peak around 110 – 120 K). By taking into account the entropic contribution to the free energy at 110-120 K (S=205.138 J K^{-1} mol^{-1} from the database[52]), 0.5-0.6 eV of the adsorption energy in our results are reasonable. This value is between that on clean surface and O1-substituted surface. It should be noted that considering the lack of van der Waals interactions in our calculations and the impurities left on Ta_3N_5 nanoparticle in real system, it is difficult to compare the adsorption energy directly. However, investigation of the surface reaction on model system is in general the basis for the design of catalysts. Thus, we focused on the discussion comparing clean surface and O-substituted surface using the model system.

Table 1. (a)Calculated adsorption energy for Pauling-type or Griffiths-type O_2 adsorptions. The 'site' column shows the positions of O_2 adsorption shown in Figure 1(d). In middle column, 'style', shows adsorption type, G means Griffiths-type structure and P means Pauling-type structure. (b)Calculated adsorption energy for Yeager-type structure together with the adsorbed Ta-Ta length in the middle column.

(a) Clean surface

site	style	E_{ad} (eV)
A	G	0.00
B	G	-0.04

O1-substituted surface

site	style	E_{ad} (eV)
A	G	-0.99
B	P	-0.55
C	P	-0.55
E	G	-0.95
F	G	-1.02

O2-substituted surface

site	style	E_{ad} (eV)
A	G	-1.83
B	P	-0.82
C	P	-0.71
D	G	-1.71
E	G	-1.55
F	G	-1.67

(b) Clean surface

site	$d_{Ta\text{-}Ta}$ (Å)	E_{ad} (eV)
A-B	4.06	0.00
A-C	4.03	-0.04
B-D	3.38	-0.06
C-D	3.19	0.05

O1-substituted surface

site	$d_{Ta\text{-}Ta}$ (Å)	E_{ad} (eV)
B-D	3.56	-0.85
C-D	3.37	-0.71
D-E	4.04	-0.54
D-F	3.95	-0.63
E-F	4.04	-0.67
A-E	3.38	-0.87
A-B	4.04	-0.66
A-C	4.07	-0.55
B-F	3.27	-0.93
B-C	4.20	-0.54
C-E	3.31	-0.82

O2-substituted surface

site	$d_{Ta\text{-}Ta}$ (Å)	E_{ad} (eV)
B-D	3.64	-2.00
C-D	3.35	-1.71
D-E	4.00	-0.69
D-F	3.89	-0.70
E-F	4.03	-1.06
A-E	3.34	-1.35
A-B	3.99	-0.52
A-C	4.06	-0.56
B-F	3.23	-1.43
B-C	4.17	-1.03
C-E	3.36	-1.48
A-F	3.32	-1.58

3.2 Mechanism for the ORR on Clean and O-substituted Surfaces

In this section, we examine the mechanism for the ORR starting from Yeager-type and Griffiths-type adsorption on clean and O-substituted surfaces. As an example of an O-substituted surface, the O2-substituted surface (Fig. 1(c)) was selected because the effect of O-substitution is stronger on the

O2-substituted surface than that on the O1-substituted surface. The active sites for the oxygen reduction reaction were determined to be B-D site in Yeager-type adsorption and A site in Griffiths-type adsorption because the adsorption energy on these two sites are strongest among other sites (see Table 1, the data about O2-substituted surface).

Both 4-electron and 2-electron reactions on clean and O2-substituted surfaces were considered as mechanisms for the ORR. The 4-electron and 2-electron reactions are:

$O_2 + 4H^+ + 4e^- \rightarrow 2H_2O$ (4-electron)

$O_2 + 2H^+ + 2e^- \rightarrow H_2O_2$. (2-electron)

It has remained controversial which reaction occurs, even on a Pt surface, although the 4-electron reaction is considered to be favourable. Therefore, we examined the possibilities of both reactions on clean and O2-substituted Ta_3N_5 surfaces. The reaction difference between 4-electron and 2-electron reaction is whether O-O bond breaking occurs or not. We assumed that O-O bond breaking is likely to occur when oxygen molecule adsorbs between two Ta sites. By contraries, oxygen reduction without O-O bond breaking is likely to proceed when oxygen adsorb on one Ta sites. Based on this assumption, the energy diagram of 4-electron reaction from Yeager-type oxygen adsorption and 2-electron reaction from Griffiths-type oxygen adsorption were calculated. The energy diagrams of 4-electron and 2-electron reactions on clean and O2-substituted surfaces were examined by the frequently used method for the electrochemical reaction originally suggested by Nørskov et al[2]. Here, we treat the energy of ($H^+ + e^-$) to be equal to that of 1/2 H_2 to take into account the reaction under the condition of 0.0 V vs. SHE (standard hydrogen electrode). The entropic effect and zero-point energy (ZPE) correction were included for the calculation of H_2 and O_2 molecules using the database[52]. For the adsorbed species, the entropic effect can be ignored and the only ZPE correction of 0.07 eV for O* and 0.3 eV for OH* was added following to ref. 2. For a water-adsorbed system, ZPE is estimated to be 0.6 eV, which is twice that of an OH-adsorbed system. ZPE corrections in our system can be justified because they are originated to the O-H vibration and not heavily depending on the kinds of the surfaces. For example, ZPE corrections were calculated on TiO_2 (110) to be 0.05 eV for O*, 0.35 eV for OH* and 0.7 eV for OH_2*[53]. On α-Fe_2O_3 system, they are 0.04 eV for O*, 0.37 eV for OH* and 0.67 eV for OH_2*[54]. The difference among the system is within 0.1 eV. The adsorption energies of intermediates were calculated using this method with basis set superposition error (BSSE) and dipole corrections. To consider the water affinity effect, three water molecules were added for the surface including OH* and H_2O* species. Here we use "*" to denote an adsorbed species.

3.2.1 Reaction Mechanism Starting from Yeager-type Adsorption

The mechanism for the ORR on a clean surface starting from Yeager-type oxygen adsorption for the 4-electron reaction was examined first. The calculated energy diagram and the structures of the adsorbed species at each step are shown in Figures 4 and 5, respectively. Because O_2 itself cannot adsorb onto the clean surface, oxygen first adsorbs together with (H^++e^-) and then forms OOH* (step 2). The adsorbed O-O bond is broken with the second (H^++e^-) transfer to form O* and H_2O* (step 3) without an energy barrier. H_2O then desorbs from the surface and the O* species (step 4) remains. Following the subsequent (H^++e^-) transfer, H_2O* is formed again (step 6). The second H_2O desorption is the rate-determining step that requires an energy of 1.28 eV (step 7). During the geometry optimizations, the reaction path forming OH* and OH* after the second (H^++e^-) transfer cannot be found in our calculations. The second H_2O desorption energy is higher compared to the first H_2O desorption energy. Z. Zou et al investigated the water adsorption and dissociation on Ta_3N_5 (100) surface by DFT calculations[41]. They claimed the dangling bond strongly adsorb water on surface. Similar to this mechanism, in the present study, the clean surface with adsorbed O* is positively charged (Mulliken charge of adsorbed O* is -0.40), which means the reduction of dangling bond on the surface. This leads to the decrease of the first H_2O desorption energy. From our calculations, the bottleneck for the reaction is water desorption at the last step. It should be stressed that O_2 cannot adsorb without (H^++e^-) on the clean surface; therefore, almost all the active sites may be covered by other molecular species such as H_2O* and OH*. The adsorption of these species can also decrease the catalytic activity.

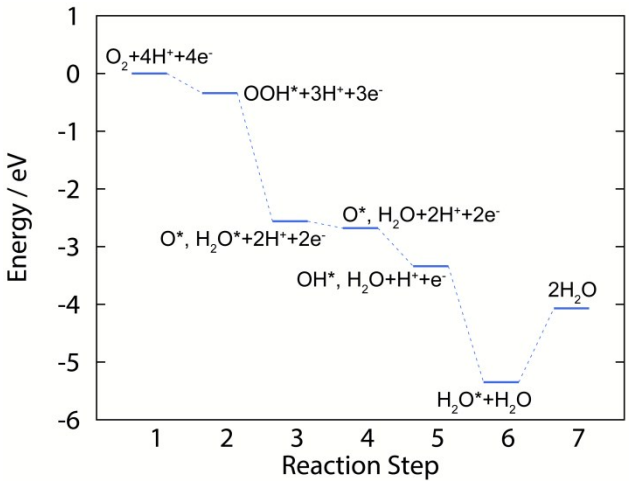

Figure 4. Calculated energy diagram of ORR on clean surface. The formation energy of H_2O at step 7 is calculated in the gas phase model to be 4.07 eV

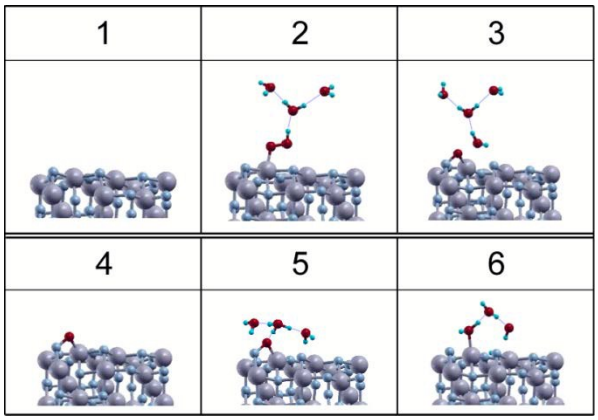

Figure 5. Structures of adsorbed species at each reaction step of ORR. The number corresponds to the number of reaction step in Fig. 4.

Next, the mechanism for the ORR on an O2-substituted surface starting from Yeager-type oxygen adsorption for the 4-

electoron reaction was examined. The calculated energy diagram and structures of the adsorbed species are shown in Figures 6 and 7, respectively. An oxygen molecule first adsorbs strongly on the O2-substituted surface. The O-O bond then breaks when (H^++e^-) transfers to form O* and OH* (step 3) without any energy barrier. After consecutive (H^++e^-) transfer, O* and H_2O* is produced (step 4). Energy of 0.82 eV is required for the first water desorption (from step 4 to step 5). The second water desorption (from step 6 to step 8) requires the energy of 0.94 eV. From our calculations, the rate determining step for the reaction on an O2-substituted surface is also the water desorption. The energy barrier for the water desorption is less than that for a clean surface. Therefore, the O2-substituted surface has higher ORR activity. However, the stable OH* and H_2O* species decrease the catalytic activity, as shown by the dashed line in Figure 6 (step 4 and step 5).

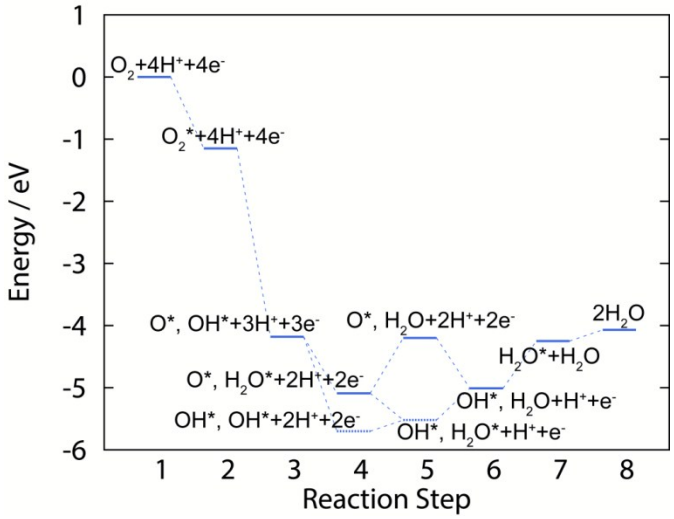

Figure 6. Calculated energy diagram of ORR on O2-substituted surface.

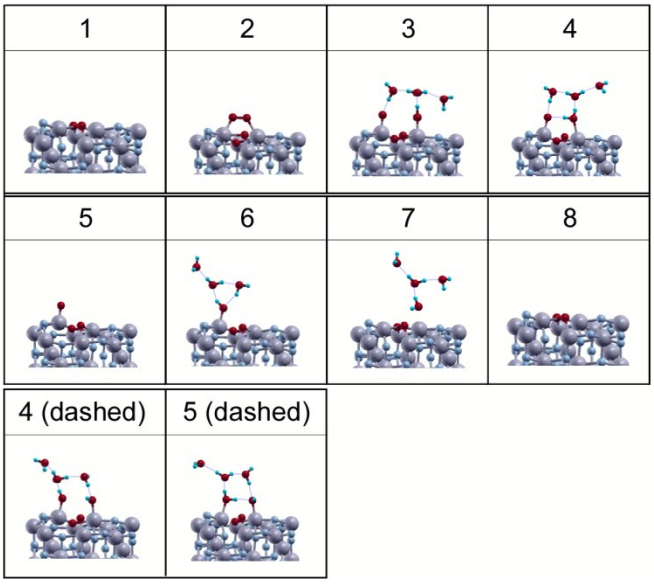

Figure 7. Structures of adsorbed species at each reaction step of ORR. The number corresponds to the number of reaction step in Fig. 6.

3.2.2. Reaction Mechanism Starting from Griffiths-type Adsorption

An energy diagram was next calculated for the ORR which starts from Griffiths-type adsorption for the 2-electron reaction. The calculated energy diagram is shown in Figure 8 together with the structures of adsorbed species on the O2-substituted surface. The red and blue lines represent the energy for the ORR on clean and O2-substituted surfaces, respectively. On the clean surface, oxygen adsorbs onto the surface with (H^++e^-) (step 3) and the reaction proceeds to generate H_2O_2* (step 4). The H_2O_2 desorption energy is approximately 0.84 eV (step 5). On the O2-substituted surface, oxygen adsorbs strongly onto the surface (step 2) and OOH* is generated (step 3). An energy of 0.81 eV is required from OOH* to produce desorbed H_2O_2 (step 4). Our calculations indicate that the 2-electron reaction proceeds on the O2-substituted surface rather than on the clean surface because of the stronger O_2 adsorption energy and slightly smaller H_2O_2 desorption energy on O2-substituted surface. Compared with experimental data, the H_2O_2 formation energy of 0.59 eV is relatively smaller than that in the database[52] (1.25 eV) because the energy is calculated in a gas phase model in the present study. Therefore, we inserted experimental data for step 5 to elucidate that H_2O_2 production proceeds with the little energy barrier. By comparing the 4-electron and 2-electron reactions, the smaller energy barrier on the 2-electron reaction shows that the main product on the Ta_3N_5(100) surface is H_2O_2, which is in good agreement with the experimental report that suggests hydrogen peroxide is obtained on metal oxide and nitride catalysts[24].

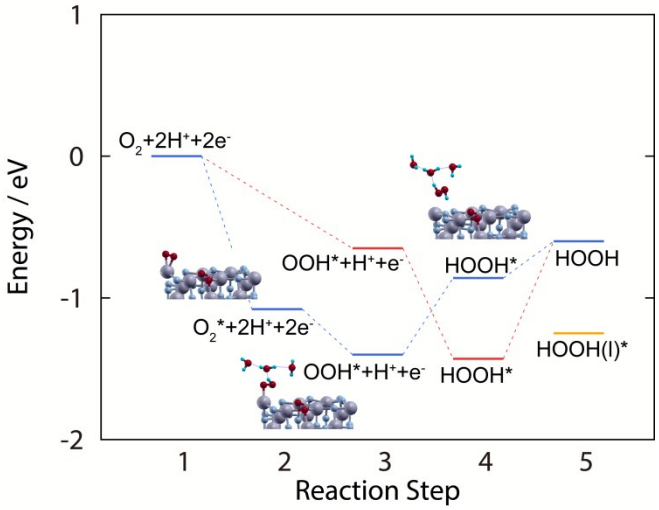

Figure 8. Calculated energy diagram of H_2O_2 production on clean and O2-substituted surface. The red line shows the reaction on clean surface and blue line shows the reaction on O2-substituted surface. Corresponding structures are shown as the snapshot of each reaction step on O2-substituted surface. The yellow line at step 5 is derived experimental formation energy of H_2O_2(l)[54].

3.3 Difference in Catalytic Activity Between Clean and O-substituted Surfaces

A comparison of the reaction on clean and O2-substituted surfaces indicates that the O2-substituted surface has higher catalytic activity than the clean surface. The small adsorption energy of O_2 may be the bottleneck for the 4-electron and 2-electron reactions on a clean surface. OH and H_2O adsorb

strongly onto the clean surface; therefore, the surface sites are covered by water, which suppresses O_2 adsorption. On the other hand, O_2 adsorbs strongly onto the O2-substituted surface and the probability of starting the reaction is higher than on the clean surface. In addition, the H_2O and H_2O_2 desorption energy is smaller than on the clean surface. A summary of the energy diagram calculations indicates that the O2-substituted surface has higher catalytic activity because of strong O_2 adsorption energy and smaller H_2O_2 desorption energy. It should be noted that O2-substituted surface is one model system for the oxidized surface. Considering O_2 adsorption energy reported by experiment is between that on clean surface and O1-substituted surface, oxygen reduction reaction possibly occurs at partially oxidized Ta_3N_5 surface.

3.4 Origin of Catalytic Activity on the Ta_3N_5(100) surface

From the discussions in sections 3.2 and 3.3, the difference of the catalytic activity for the ORR on clean and O2-substituted surfaces is determined to be the O_2 adsorption energy and H_2O/H_2O_2 desorption energy. Our previous calculations of the density of states (DOS) for clean and O-substituted surfaces show that an impurity state appears between the CB and VB on the O-substituted surface, which allows O_2 adsorption[40]. The impurity state can attack O_2 π^* anti-bonding orbitals to weaken the O-O bonds, which leads to O_2 chemisorption on the surface. The ORR catalytic activity is significantly related to the O_2 adsorption energy; therefore, the impurity state is essential for the catalytic activity of non-conductive transition metal oxides or nitrides. In particular, when the π^* orbital of O_2 is located above the VB in a semiconductor, the transfer of electrons from the semiconductor surface to O_2 molecule is difficult without the impurity state. In this context, the adsorption (binding) energies of O_2 and OH on clean and O-substituted surfaces were examined, and the calculated energies are given in Table 2. The O_2 adsorption energy changed significantly from 0.0 eV (on the clean surface) to -2.0 eV (on the O2-substituted surface), and the adsorption energy of OH changed from -2.3 eV (on the clean surface) to -3.3 eV (on the O2-substituted surface). Thus, OH interacts strongly even on the clean surface. The variety of O_2 adsorption energies contributes to the difference in catalytic activity between the clean and O-substituted surfaces and the strong binding energy of OH leads to the endothermic water desorption energy even on the O2-substituted surface. Finally, effect of Hubbard *U* parameter on the binding energy was investigated. The parameter (*U*=5.0 eV) was selected to recover the experimental band gap (2.1 eV[39]) in the bulk system. The calculated O_2 adsorption energies were -0.71 eV and -1.21 eV, and OH binding energies were -2.7 eV and -2.9 eV on O1-substituted and O2-substituted surfaces respectively. All the values are reduced and Hubbard *U* correction affects the energy diagram. The decrease rate of the O_2 adsorption energies are 21 % and 40 % and the decrease rate of the OH binding energies are 21 % and 40 % on O1-substituted and O2-substituted surfaces respectively. Because the adsorption of O_2 needs the electron donation from the surface, it strongly depends on the level of the impurity states easily affected by the Hubbard *U* correction. On contrary, OH binding energy dependence on the correction is relatively small. Thus, the energy from OH* (step 6 in Figure 6) to produce water (step 8 in Figure 6) on O2-substituted surface may not be largely affected by Hubbard *U* corrections.

Table 2. Calculated adsorption energy of O_2 and OH with Ta_3N_5 (100) surfaces.

	O_2*	OH*
clean surface	-0.1 eV	-2.3 eV
O1-substituted surface	-0.9 eV	-3.0 eV
O2-substituted surface	-2.0 eV	-3.3 eV

3.5 Strategy to Control ORR Activity

From discussions in the last subsections, a strategy for the higher ORR activity can be achieved by controlling the energy level of the impurity state. Therefore, the energy levels of the O2-substituted Ta_3N_5 surface and reactant molecules (O_2, OH) were analysed by calculation of the DOS. The relative energies of O_2 and OH to the O2-substituted surface are calculated by setting the same vacuum level. The DOS calculated for Ta_3N_5, O_2 and OH are shown in Fig. 9(a). The distribution of the impurity state for Ta_3N_5 (red line) crosses the Fermi energy. The singly occupied molecular orbital (SOMO) of O_2 (blue line) has an energy peak at -2.3 eV and the SOMO of OH (yellow line) has an energy peak at -1.2 eV. By considering the interaction with the Ta impurity state, the energy peak for the SOMO of OH is closer than that for O2 (see Fig. 9(b)). This means that interaction between the impurity state and SOMO of OH is strong, which leads to the stable adsorption of OH*. Therefore, the O_2 and OH adsorption energies can be controlled by changing the energy level of the impurity state.

Let us consider how to improve the ORR activity. To enable O_2 adsorption on the surface, the impurity state must be located above the SOMO level of O_2. In contrast, to decrease the OH binding energy, the impurity state is better located far away from the SOMO level of OH. Therefore, the target energy for the impurity state is above the SOMO level of O_2 and under the SOMO level of OH. Thus, to improve the ORR activity, we propose the (co)doping of carbon atoms in accordance with oxygen. O-substitution on nitrides donates electron that makes the impurity state below the CB that can act as d band in metal catalysts. On contrary, C-substitution donates hole that undershifts the energy level of the impurity state. Thus, C-substitution could possibly weaken the binding energy of OH while keeping the energy of the impurity state above the SOMO level of O_2. This is consistent with experimental results for the order of catalytic activity among Ta_3N_5, TaNO and TaCNO[23,32], where TaCNO has the highest activity; TaCNO>TaNO>Ta_3N_5.

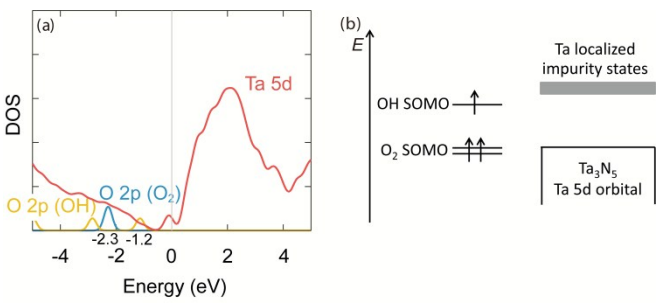

Figure 9 (a) Calculated DOS of Ta_3N_5 O2-substituted surface, isolated O_2 and OH are shown. The red line shows the contribution of Ta 5d orbital in Ta_3N_5, blue line shows the contribution of O 2p orbital in O_2, the yellow line shows the contribution of O 2p orbital in OH respectively. The energy peak of -2.3 eV in blue line corresponds to O_2 SOMO orbital and the energy peak of -1.2 eV in yellow line corresponds to OH SOMO orbital. (b) A schematic picture of relative energy of Ta_3N_5, O_2 and OH is shown. The impurity state of Ta_3N_5 has higher energy than OH and O_2.

Conclusions

The reaction mechanism for the ORR on Ta_3N_5(100) surfaces has been examined theoretically. Clean and O-substituted surfaces were modelled to examine the relationship between the surface structures and catalytic activities. First, the adsorption structures and energies of oxygen were examined to clarify the mechanism for the ORR. From our calculations, it can be concluded that there are two possible adsorption structures of oxygen: Yeager-type and Griffiths-type. Energy diagrams for both the 4-electron and 2-electron reactions on both clean and O-substituted surfaces were then examined. By comparing each reaction, H_2O/H_2O_2 desorption was determined as the rate-determining step on both clean and O2-substituted surfaces. The difference in the catalytic activity of the clean and O2-substituted surfaces is mainly due to O_2 adsorption energy, and the O2-substituted surface is considered to have higher catalytic activity. Finally, we analysed the energy level of the impurity state for the O2-substituted surface and the orbital energies of adsorbed species. Based on the results, we have demonstrated the possibility of catalytic activity control by changing the surface structures. Control of the energy of the impurity state just above the SOMO level of O_2 is an effective way to improve catalytic activity for the ORR, and we have suggested C-doped $Ta_3N_{5-x}O_x$ as candidates for higher catalytic ORR activity. The concepts presented here are fundamental and useful for the design of new materials with higher catalytic activities.

Acknowledgements

This work was supported in part by the Strategic Programs for Innovative Research (SPIRE), MEXT, and the Computational Materials Science Initiative (CMSI), and Grants-in-Aid for Scientific Researches from Ministry of Education, Culture, Sports, Science and Technology, Japan. E. W. was supported by Japan Society for the Promotion of Science through Program for Leading Graduate Schools (MERIT)

Notes and references

1 L. Carrette, K. a Friedrich and U. Stimming, *Fuel Cells*, 2001, **1**, 5.
2 J. K. Nørskov, J. Rossmeisl, a. Logadottir, L. Lindqvist, J. R. Kitchin, T. Bligaard and H. Jónsson, *J. Phys. Chem. B*, 2004, **108**, 17886.
3 V. Tripković, E. Skúlason, S. Siahrostami, J. K. Nørskov and J. Rossmeisl, *Electrochim. Acta*, 2010, **55**, 7975.
4 M. J. Janik, C. D. Taylor and M. Neurock, *J. Electrochem. Soc.*, 2009, **156**, B126.
5 A. Panchenko, M. T. M. Koper, T. E. Shubina, S. J. Mitchell and E. Roduner, *J. Electrochem. Soc.*, 2004, **151**, A2016.
6 F. Jaouen, E. Proietti, M. Lefèvre, R. Chenitz, J.-P. Dodelet, G. Wu, H. T. Chung, C. M. Johnston and P. Zelenay, *Energy Environ. Sci.*, 2011, **4**, 114.
7 U. Paulus, A. Wokaun, G. Scherer, T. Schmidt, V. Stamenkovic, V. Radmilovic, N. Markovic, and P. Ross, *J. Phys. Chem. B*, 2002, **106**, 4181.
8 J. Greeley, I. E. Stephens, A. S. Bondarenko, T. P. Johansson, H. A. Hansen, T. F. Jaramillo, J. Rossmeisl, I. Chorkendorff, and J. K. Nørskov, *Nat. Chem*, 2009, **1**, 552–6.
9 K. Kuttiyiel, K. Sasaki, Y. Choi, D. Su, P. Liu, and R. Adzic, *Nano Lett.*, 2012, **12**, 6266.
10 W. Yang, Y. Wang, J. Li, and X. Yang, *Energy Environ. Sci*., 2009, **3**, 144.
11 X. Chen, S. Sun, X. Wang, F. Li and D. Xia, *J. Phys. Chem. C*, 2012, **116**, 22737.
12 G. Wu, K. L. More, C. M. Johnston and P. Zelenay, *Science*, 2011, **332**, 443.
13 S. Gupta, D. Tryk, I. Bae, W. Aldred and E. Yeager, *J. Appl. Electrochem.*, 1989, **19**, 19.
14 R. Jasinski, *Nature*, 1964, **201**, 1212.
15 M. Kaukonen, R. Kujala and E. Kauppinen, *J. Phys. Chem. C*, 2012, **116**, 632.
16 B. Shan and K. Cho, *Chem. Phys. Lett.*, 2010, **492**, 131.
17 H. Niwa, K. Horiba, Y. Harada, M. Oshima, T. Ikeda, K. Terakura, J. Ozaki and S. Miyata, *J. Power Sources*, 2009, **187**, 93.
18 K. Gong, F. Du, Z. Xia, M. Durstock and L. Dai, *Science*, 2009, **323**, 760.
19 M. Lefèvre, E. Proietti, F. Jaouen and J.-P. Dodelet, *Science*, 2009, **324**, 71.
20 Y. Okamoto, *J. Phys. Chem. C*, 2008, **112**, 5888.
21 A. Lyalin, A. Nakayama, K. Uosaki and T. Taketsugu, *J. Phys. Chem. C*, 2013, **117**, 21359.
22 J. Suntivich, H. A. Gasteiger, N. Yabuuchi, H. Nakanishi, J. B. Goodenough and Y. Shao-Horn, *Nat. Chem.*, 2011, **3**, 546.
23 A. Ishihara, Y. Ohgi, K. Matsuzawa, S. Mitsushima and K. Ota, *Electrochim. Acta*, 2010, **55**, 8005.
24 R. Ohnishi, K. Takanabe, M. Katayama, J. Kubota and K. Domen, *J. Phys. Chem. C*, 2013, **117**, 496.
25 A. Ishihara, M. Tamura, K. Matsuzawa, S. Mitsushima and K. Ota, *Electrochim. Acta*, 2010, **55**, 7581.
26 R. Ohnishi, M. Katayama, K. Takanabe, J. Kubota and K. Domen, *Electrochim. Acta*, 2010, **55**, 5393.
27 A. Ishihara, Y. Shibata, S. Mitsushima and K. Ota, *J. Electrochem. Soc.*, 2008, **155**, B400.
28 A. Ishihara, S. Doi, S. Mitsushima and K. Ota, *Electrochim. Acta*, 2008, **53**, 5442.
29 R. Ohnishi, Y. Takahashi, A. Takagaki, J. Kubota and K. Domen, *Chem. Lett.*, 2008, **37**, 838.
30 S. Doi, A. Ishihara, S. Mitsushima, N. Kamiya and K. Ota, *J. Electrochem. Soc.*, 2007, **154**, B362.
31 J.-H. Kim, A. Ishihara, S. Mitsushima, N. Kamiya and K.-I. Ota, *Electrochim. Acta*, 2007, **52**, 2492.
32 A. Ishihara, K. Lee, S. Doi, S. Mitsushima, N. Kamiya, M. Hara, K. Domen, K. Fukuda and K. Ota, *Electrochem. Solid-State Lett.*, 2005, **8**, A201.
33 J. Seo, D. Cha, K. Takanabe, J. Kubota and K. Domen, *ACS Catal.*, 2013, **3**, 2181.
34 J. Seo, D. Cha, K. Takanabe, J. Kubota and K. Domen, *Chem. Commun. (Camb).*, 2012, **48**, 9074.
35 K. Ota, Y. Ohgi, K.-D. Nam, K. Matsuzawa, S. Mitsushima and A. Ishihara, *J. Power Sources*, 2011, **196**, 5256.

36 K. Maeda and K. Domen, *J. Phys. Chem. C*, 2007, **111**, 7851.
37 M. Hara, G. Hitoki, T. Takata, J. N. Kondo, H. Kobayashi and K. Domen, *Catal. Today*, 2003, **78**, 555.
38 G. Hitoki, A. Ishikawa, T. Takata, J. N. Kondo, M. Hara and K. Domen, *Chem. Lett.*, 2002, **31**, 736.
39 W.-J. Chun, A. Ishikawa, H. Fujisawa, T. Takata, J. N. Kondo, M. Hara, M. Kawai, Y. Matsumoto and K. Domen, *J. Phys. Chem. B*, 2003, **107**, 1798.
40 E. Watanabe, H. Ushiyama and K. Yamashita, *Chem. Phys. Lett.*, 2013, **561-562**, 57.
41 J. Wang, W. Luo, J. Feng, L. Zhang, Z. Li and Z. Zou, *Phys. Chem. Chem. Phys*., 2013, **15**, 16054.
42 J. Wang, T. Fang, L. Zhang, J. Feng, Z. Li and Z. Zou, *J. Catal.*, 2014, **309**, 291.
43 J. M. Soler, E. Artacho, J. D. Gale, A. García, J. Junquera, P. Ordejón and D. Sánchez-Portal, *J. Phys. Condens. Matter*, 2002, **14**, 2745.
44 B. Hammer, L. Hansen and J. Nørskov, *Phys. Rev. B*, 1999, **59**, 7413.
45 J. Junquera, Ó. Paz, D. Sánchez-Portal and E. Artacho, *Phys. Rev. B*, 2001, **64**, 1.
46 N. Troullier and J. L. Martins, *Phys. Rev. B*, 1991, **43**, 1993.
47 D. Sheppard, R. Terrell and G. Henkelman, *J. Chem. Phys.*, 2008, **128**, 134106.
48 N. González-García, J. Pu, À. González-Lafont, J. M. Lluch and D. G. Truhlar, *J. Chem. Theory Comput.*, 2006, **2**, 895.
49 T. Ohto, I. Rungger, K. Yamashita, H. Nakamura and S. Sanvito, *Phys. Rev. B*, 2013, **87**, 205439.
50 N. E. Brese, M. O'Keeffe, P. Rauch and F. J. DiSalvo, *Acta Crystallogr. Sect. C Cryst. Struct. Commun*., 1991, **47**, 2291.
51 H. J. Monkhorst and J. D. Pack, *Phys. Rev. B*, 1976, **13**, 5188.
52 P. W. Atkins, Physical Chemistry, 6th ed., 1998.
53 Á. Valdés, Z. Qu, G. Kroes, J. Rossmeisl, and J. Nørskov, *J. Phys. Chem. C*, 2008, **112**. 9872
54 P. Liao, J. Keith, and E. Carter, *J. Am. Chem. Soc*., 2012. **134**, 13296

